NASA TECHNICAL NOTE

NASA TN D-4334

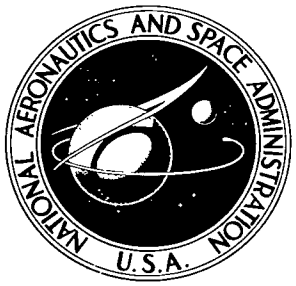

NASA TN D-4334

DISPLACEMENT OF DISINTEGRATING LIQUID JETS IN CROSSFLOW

by Frederick P. Povinelli

Lewis Research Center
Cleveland, Ohio

NATIONAL AERONAUTICS AND SPACE ADMINISTRATION • WASHINGTON, D. C. • FEBRUARY 1968

DISPLACEMENT OF DISINTEGRATING LIQUID JETS IN CROSSFLOW

By Frederick P. Povinelli

Lewis Research Center
Cleveland, Ohio

NATIONAL AERONAUTICS AND SPACE ADMINISTRATION

For sale by the Clearinghouse for Federal Scientific and Technical Information
Springfield, Virginia 22151 – CFSTI price $3.00

DISPLACEMENT OF DISINTEGRATING LIQUID JETS IN CROSSFLOW

by Frederick P. Povinelli

Lewis Research Center

SUMMARY

The displacement of three sizes of liquid jets breaking up in a crossflow was measured in a shock tube. Data were obtained for water, oxygen, n-heptane, and three glycerol-water mixtures in gas flows up to 1080 feet per second (329 m/sec). The displacement was approximately proportional to gas velocity squared and inversely proportional to jet diameter. Data were correlated with an empirical parameter. A simple model of jet displacement which includes the rate of mass removal also led to a correlation of the data.

INTRODUCTION

The breakup and displacement of liquid jets and drops accompanying perturbations in local gas velocity appear to be important mechanisms in initiating and driving the transverse mode of combustion resonance in liquid-propellant systems (ref. 1). Liquid jet breakup is of importance in atomization and vaporization processes, whereas jet displacement is of interest in mixing processes and injector design. Previously (refs. 2 to 4), the process of jet breakup in the velocity field behind a shock wave was studied, and an expression for the breakup time (ref. 4) developed. That expression was in agreement with results obtained by an entirely different experimental technique (ref. 5). The present study is concerned with the displacement of the disintegrating liquid jets of reference 4 in the flow field behind a shock wave.

Other investigators (refs. 6 and 7) have reported on the displacement of drops and jets of water breaking up behind shock waves and have concluded that predictions of displacement must include assumptions of the rate of mass removal and of the changing shape of the jet cross section, neither of which is easily defined. In this report, experimental displacement data are correlated with an empirically obtained parameter which includes time, liquid jet diameter, crossflow gas velocity, and the ratio of gas to liquid densities. The parameter corresponds to an expression derived for jet displacement

which neglects mass loss. A suggested simple model of jet displacement which considers mass loss and jet deformation led to an equally good correlation. A comparison is made between the experimental water jet data of reference 7 and the empirical correlation parameter.

Experimental displacements were measured for liquid jets of water, n-heptane, oxygen, and three glycerol-water mixtures. Jet diameters were 0.052, 0.0785, and 0.157 inch (0.132, 0.199, and 0.399 cm) and crossflow gas velocities were 210, 385, 790, and 1080 feet per second (64, 117, 241, and 329 m/sec). Liquid jet velocities ranged from about 20 to 46 feet per second (6.1 to 14.0 m/sec).

SYMBOLS

A	transverse area per unit length of jet
C	constant
C_D	drag coefficient
D_j	jet diameter before deformation
M	mass per unit length of jet
M_0	initial value of M
R_j	jet radius before deformation
r	radius of curvature of deformed liquid segment
t	time
t_b	breakup time
V_g	free-stream gas velocity
x	displacement perpendicular to jet axis referred to original jet location
α	consolidating term, $0.623\,\rho_g/\rho_l C_D$ (see appendix)
β	consolidating term, $\alpha V_g t_b$ (see appendix)
ρ_g	gas density
ρ_l	liquid density

APPARATUS AND PROCEDURE

The shock-tube apparatus (fig. 1) is described in detail in references 3 and 4.

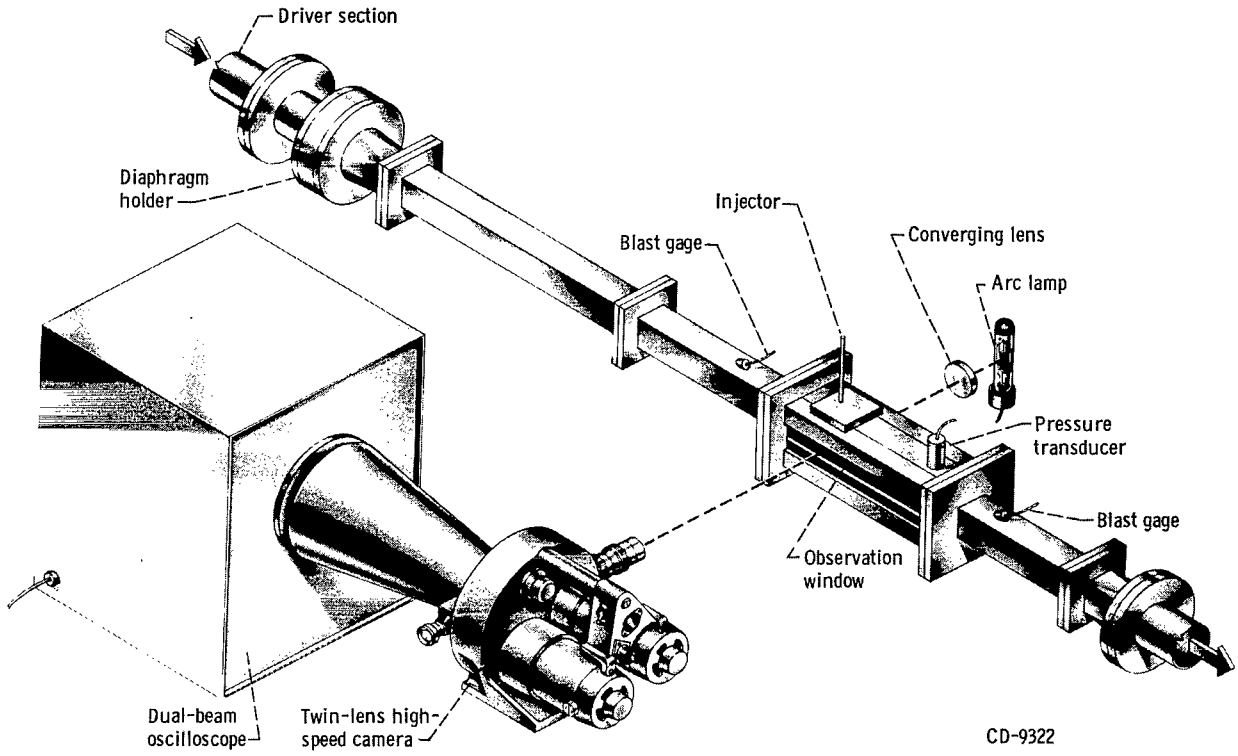

Figure 1. - Experimental setup.

Briefly, it consisted of an 8-foot- (2.4-m) long driver section, a diaphragm-piercing mechanism, and 2.72-inch- (6.91-cm) square test section with 2.72- by 14-inch (6.91- by 35.6-cm) windows. The jet axis was perpendicular to the direction of motion of the shock wave and was located 16.7 equivalent tube diameters from the diaphragm.

The motion of the deforming jet in the direction of gas flow was obtained from back-lighted streak photographs taken with a 35-millimeter shutterless motion-picture camera at a film velocity of approximately 1 inch (2.5 cm) per millisecond. The test-section window facing the camera was masked for this purpose except for an axial slit 0.1 inch (0.25 cm) wide and 14 inches (35.6 cm) long. The center of the slit was 1.36 inches (3.46 cm) below the injector face. A 50-millimeter f/2 lens was used with a demagnification of 11 at the film. Displacement of the jet leading edge was read on a film reader equipped with precision cross hairs and giving a magnification of 5. The intersection of the shock front with the jet was taken as the time reference. Displacements were measured until the jet was determined to have broken up as in reference 4. Measurement times were less than the time for reflected shocks or rarefactions to disrupt the uniform gas flow in the test section. A typical streak photograph is shown in figure 2(a) along with a corresponding framing photograph (fig. 2(b)) for comparison. Framing photo-

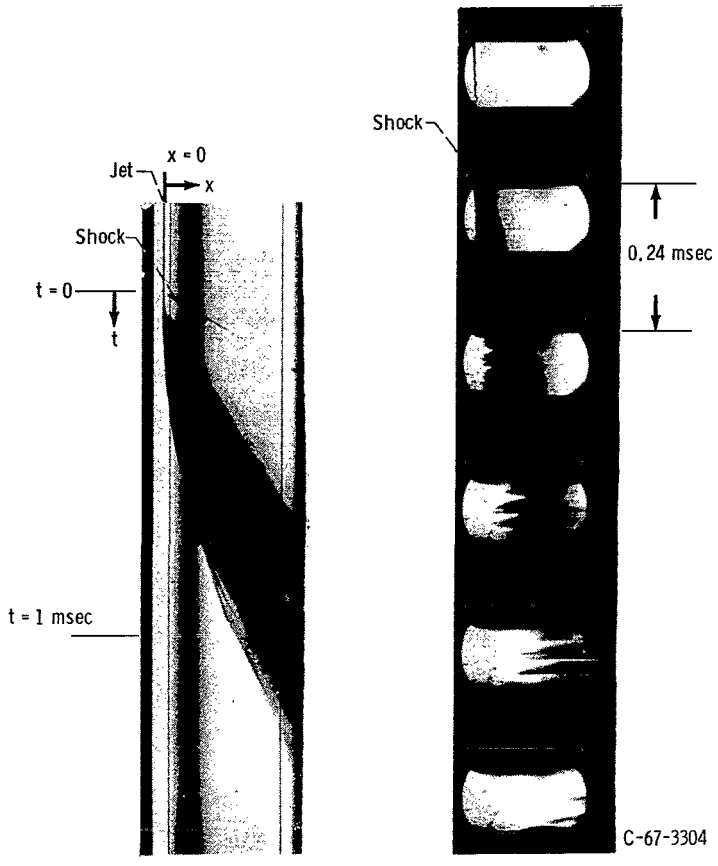

(a) Streak photograph. (b) Framing photograph.

Figure 2. - Typical photographic data of jet displacement and breakup. Gas velocity, 790 feet per second, (241 m/sec; jet diameter, 0.052 inch (0.132 cm); fluid, water.

graphs were taken with a 35-millimeter high-speed camera at a rate of approximately 2000 frames per second.

The initial pressure and temperature of the air in the test section were 1 atmosphere (1.01×10^5 N/sq m) and 70° F (294° K), respectively. Shock Mach number, shock velocity, and air velocity behind the shock wave were calculated from the initial pressure ratio by use of the one-dimensional wave equation (ref. 8). The values of shock velocity were within 5 percent of those measured from blast gages in the shock tube. For these experiments, the shock Mach number ranged from 1.115 to 1.725 and the gas velocity from 210 to 1080 feet per second (64 to 329 m/sec). The following table shows the shock tube operating conditions; liquid jet velocities ranged from 20 to 46 feet per second (6.1 to 14.0 m/sec):

Initial pressure ratio	Shock Mach number at 70° F (274° K)	Shock velocity		Gas velocity		Gas density	
		ft/sec	m/sec	ft/sec	m/sec	lb/cu ft	g/cu cm
1.68	1.115	1260	384	210	64	0.08911	1.428×10^{-3}
2.63	1.225	1384	422	385	117	.1037	1.661
7.12	1.506	1702	519	790	241	.1400	2.243
14.61	1.725	1949	594	1080	329	.1677	2.687

Three jet diameters, 0.052, 0.0785, and 0.157 inch (0.132, 0.199, and 0.399 cm) were used with each of the following liquids: water, n-heptane, oxygen, 15 weight percent glycerol in water, 58 percent glycerol, and 79 percent glycerol. Because the length-to-diameter ratios of the liquid jet injectors were at least 10, the jet was turbulent. With the exception of oxygen, all liquids were at 70° F (294° K). The oxygen was passed through a liquid-nitrogen heat exchanger and then through a vacuum-jacketed line to the injector. Properties of oxygen were evaluated at its boiling point.

RESULTS AND DISCUSSION

All the experimental data are presented graphically in figure 3. Liquid jet displacements for the various fluids are plotted as a function of time at each jet diameter and crossflow gas velocity. For several conditions, repeat runs were made to check reproducibility. These runs are shown as solid symbols in figure 3. Liquid jet velocity was found to have no effect on displacement for the small range over which it was varied.

Displacement is approximately proportional to time squared, as shown by the lines with a slope of 2 faired through the data. Fluid properties seem to have little effect on jet displacement. Close inspection of figure 3 reveals that the n-heptane data generally fall to the left of the average (a greater displacement with time) and the 15-percent-glycerol data generally fall to the right. A density effect on displacement would explain the n-heptane results but not the 15-percent-glycerol results, as shown by a comparison of densities in the following table of fluid properties; no consistent trends can be observed with surface tension or viscosity:

Liquid	Surface tension		Density		Viscosity	
	lb mass/sec^2	N/m	lb mass/cu ft	g/cu cm	lb mass/(ft)(sec)	(N)(sec)/sq m
Water	0.161	7.30×10^{-2}	62.4	1.00	6.72×10^{-4}	1.00×10^{-3}
n-Heptane	.045	2.04	42.6	.682	2.75	.409
Oxygen	.033	1.50	73.2	1.17	1.50	.223
15 Weight percent glycerol	.160	7.25	64.5	1.03	9.90	1.47
58 Weight percent glycerol	.151	6.84	71.4	1.14	6.15×10^{-3}	9.15
79 Weight percent glycerol	.147	6.66	75.0	1.20	3.49×10^{-2}	51.9

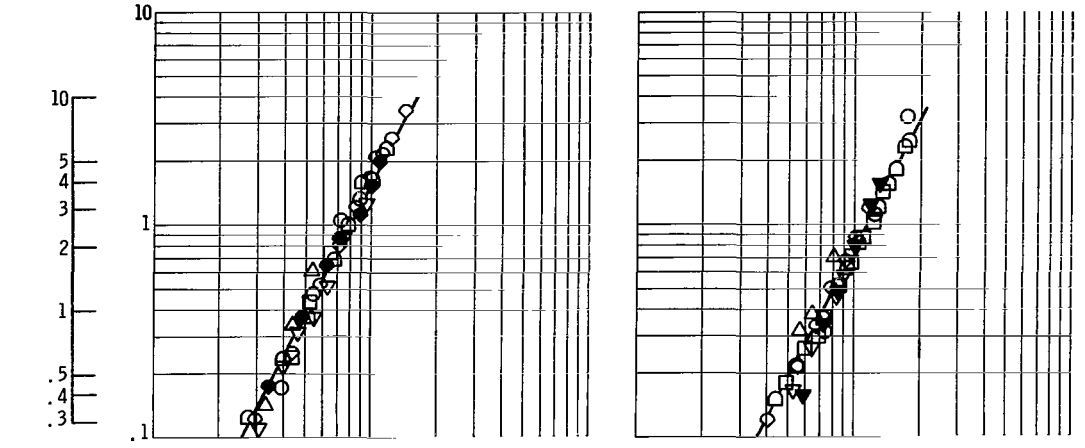

(a) Jet diameter, 0.157 inch (0.399 cm); gas velocity, 1080 feet per second (329 m/sec).

(b) Jet diameter, 0.157 inch (0.399 cm); gas velocity, 790 feet per second (241 m/sec).

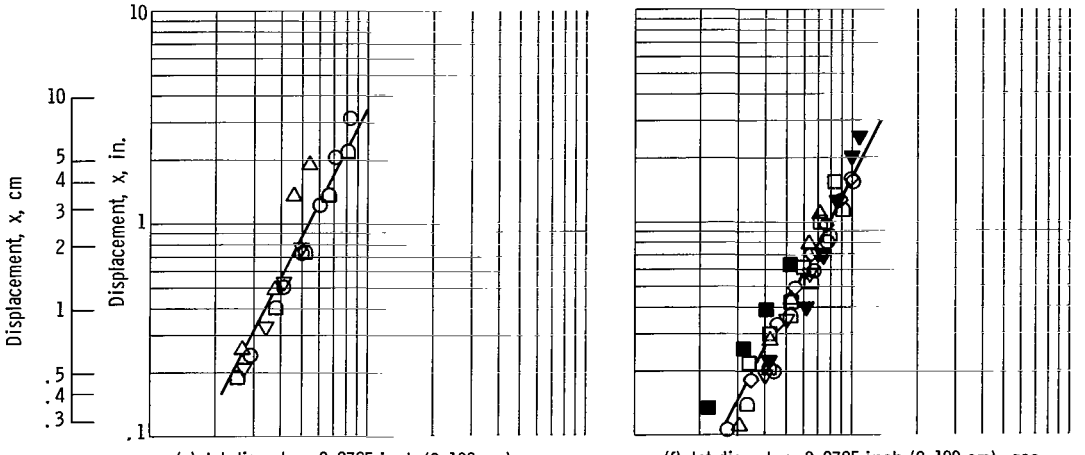

(e) Jet diameter, 0.0785 inch (0.199 cm); gas velocity, 1080 feet per second (329 m/sec).

(f) Jet diameter, 0.0785 inch (0.199 cm); gas velocity, 790 feet per second (241 m/sec).

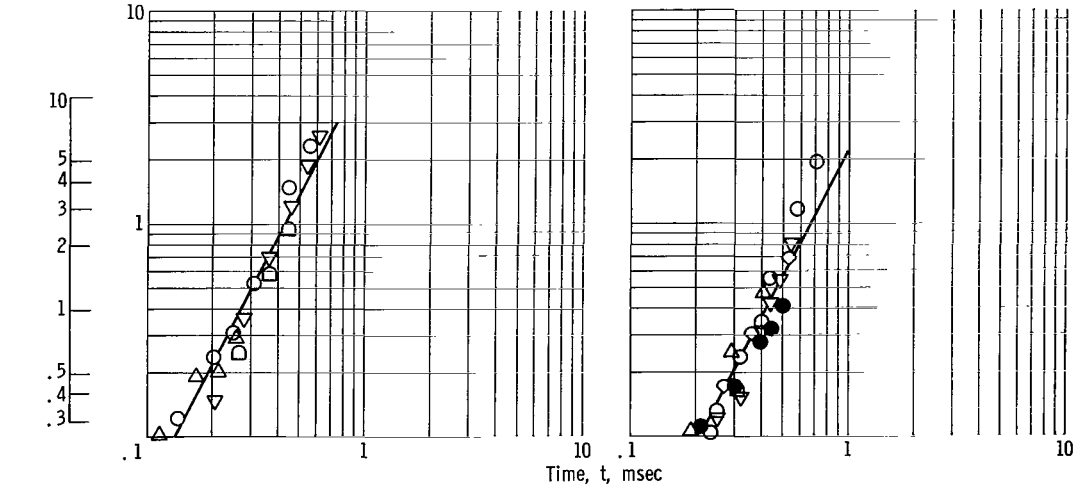

(i) Jet diameter, 0.052 inch (0.132 cm); gas velocity, 1080 feet per second (329 m/sec).

(j) Jet diameter, 0.052 inch (0.132 cm); gas velocity, 790 feet per second (241 m/sec).

Figure 3. - Effect of fluid

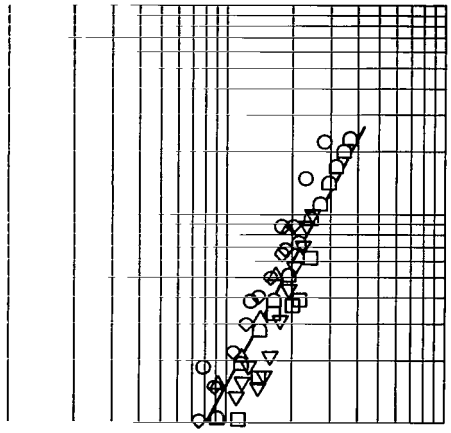

(c) Jet diameter, 0.157 inch (0.399 cm); gas velocity, 385 feet per second (117 m/sec).

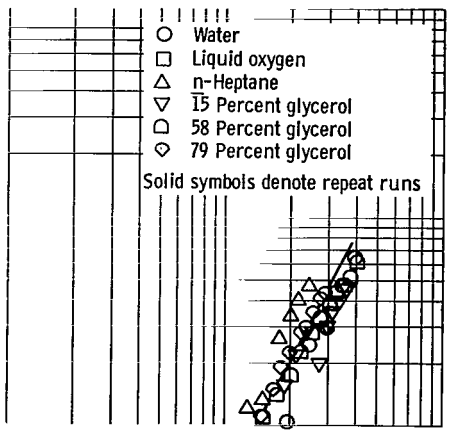

(d) Jet diameter, 0.157 inch (0.399 cm); gas velocity, 210 feet per second (64 m/sec).

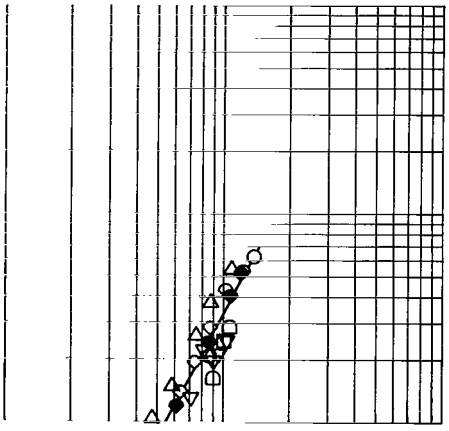

(g) Jet diameter, 0.0785 inch (0.199 cm); gas velocity, 385 feet per second (117 m/sec).

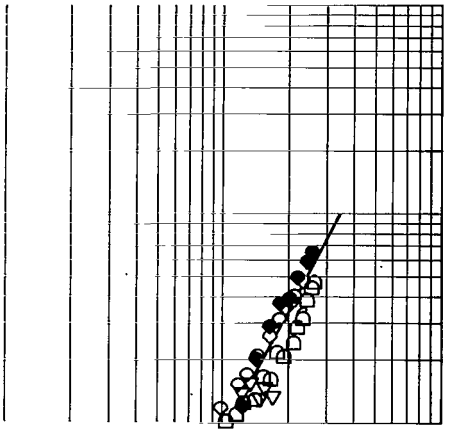

(h) Jet diameter, 0.0785 inch (0.199 cm); gas velocity, 210 feet per second (64 m/sec).

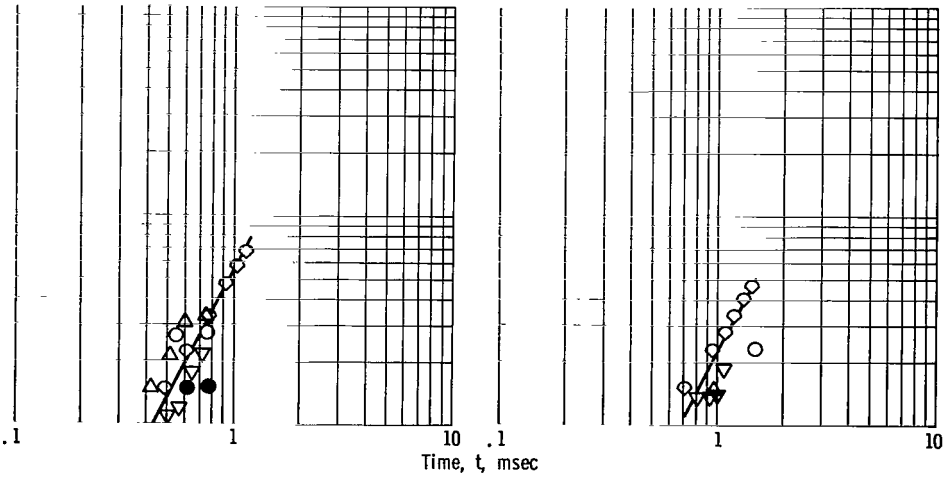

(k) Jet diameter, 0.052 inch (0.132 cm); gas velocity, 385 feet per second (117 m/sec).

(l) Jet diameter, 0.052 inch (0.132 cm); gas velocity, 210 feet per second (64 m/sec).

on jet displacement.

Some of the scatter in the data shown in figure 3, especially for lower gas velocities and smaller jet diameters, can be explained if the behavior of a disintegrating jet in crossflow is considered. The framing photograph (fig. 2(b)) shows that the jet has considerable surface roughness upon injection and deforms into segments along its entire length. In viewing the jet through an axial slit, different portions of the jet pass the slit with time. The effect which this segmented breakup has on displacement data scatter is shown in figure 4. Here, several runs are shown which indicate either a halt or a re-

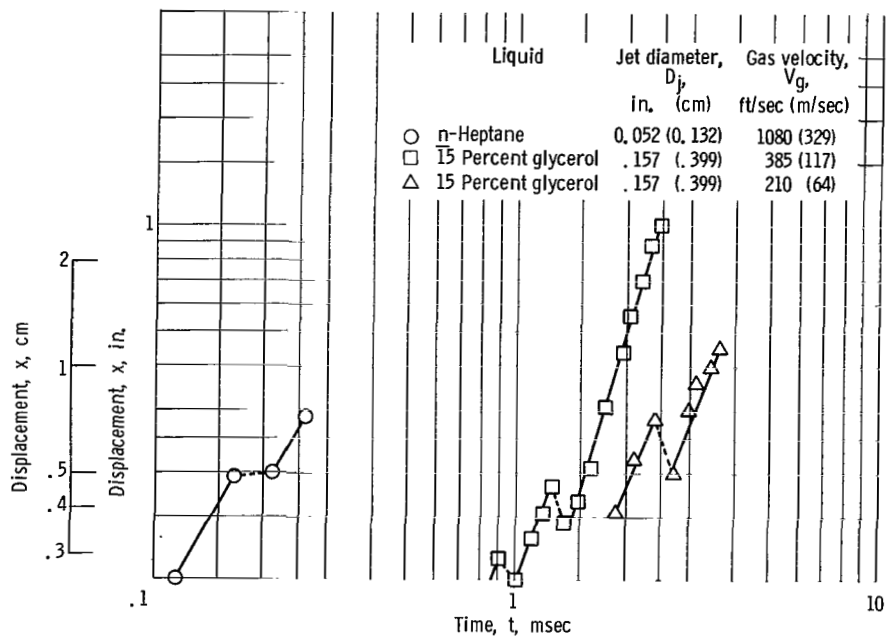

Figure 4. - Evidence of jets breaking up as series of segments. Each curve represents points taken from single streak photograph.

gression in the displacement followed by a continued increase which nearly parallels the portion before the shift. As liquid velocity increases, more halts and regressions would be expected, as more segments would pass the slit in a given time interval.

The data of figure 3 are plotted in figures 5 and 6 to show the effect of gas velocity and jet diameter, respectively, on jet displacement. Displacement is approximately proportional to gas velocity squared and is approximately inversely proportional to jet diameter.

Although the data show no obvious consistent effect of fluid density in figure 3, physically the mass or inertia of the jet would be expected to affect displacement. Also it would be expected that dynamic pressure of the gas rather than just gas velocity would affect displacement. Incorporating the preceding relations into dimensionless parameters yields

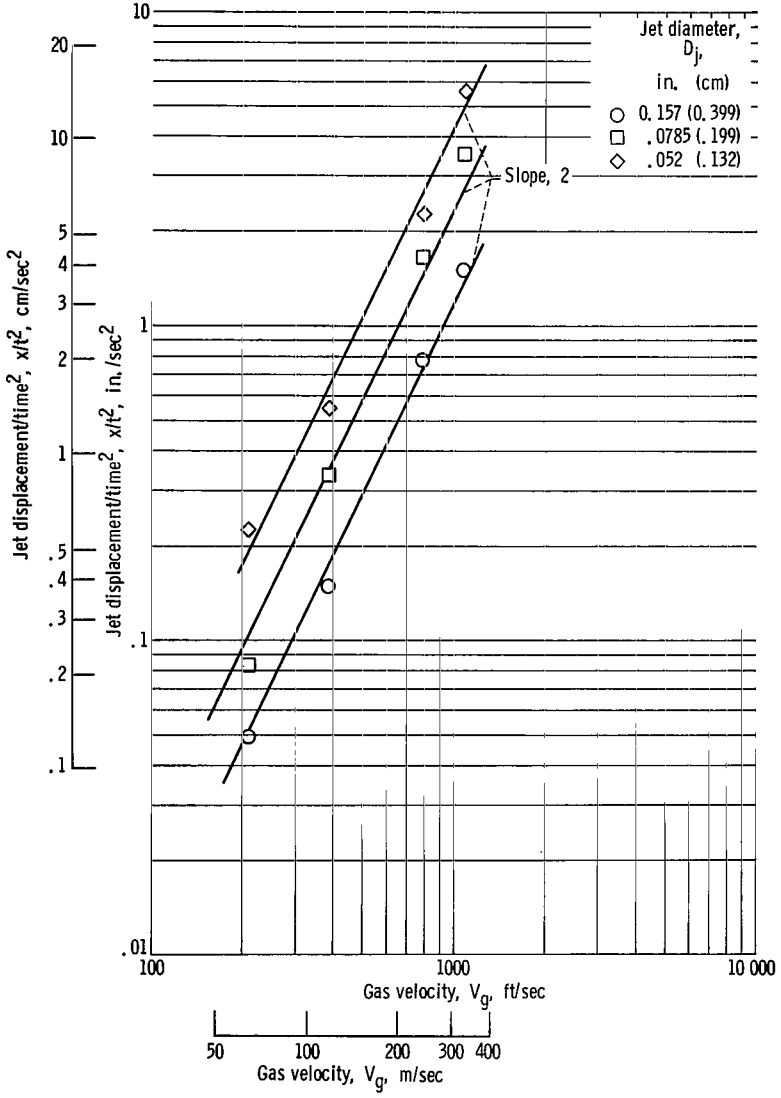

Figure 5. - Effect of gas velocity on displacement.

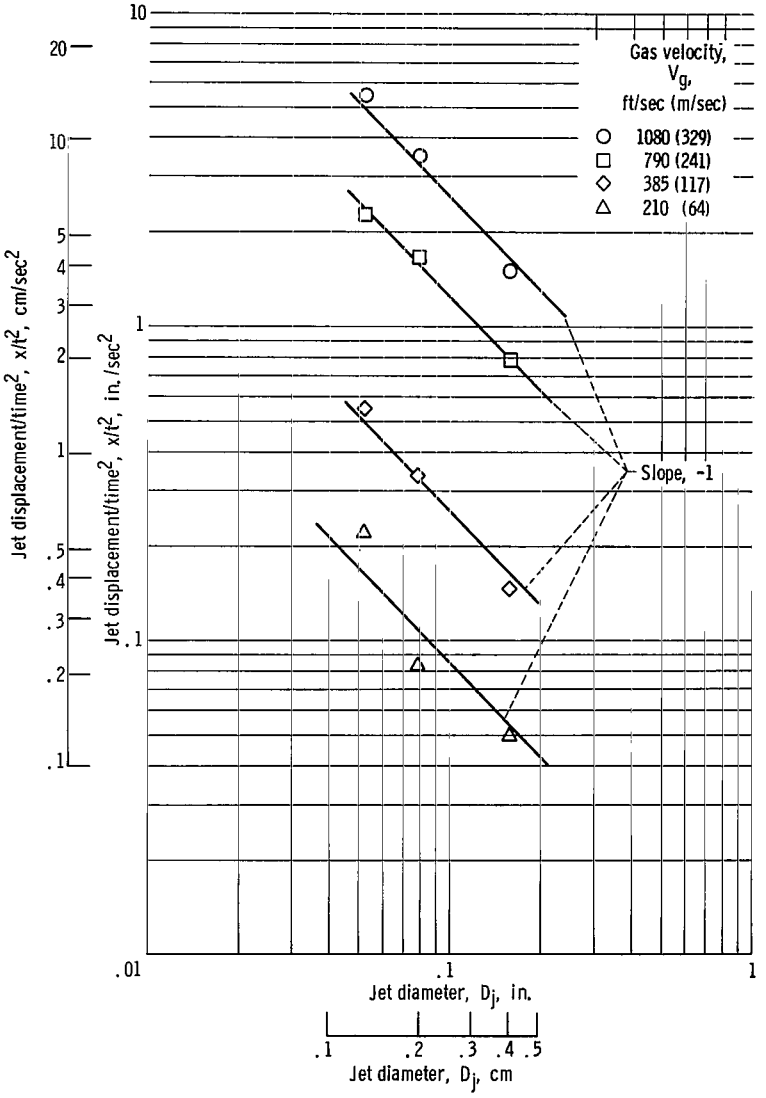

Figure 6. - Effect of jet diameter on displacement.

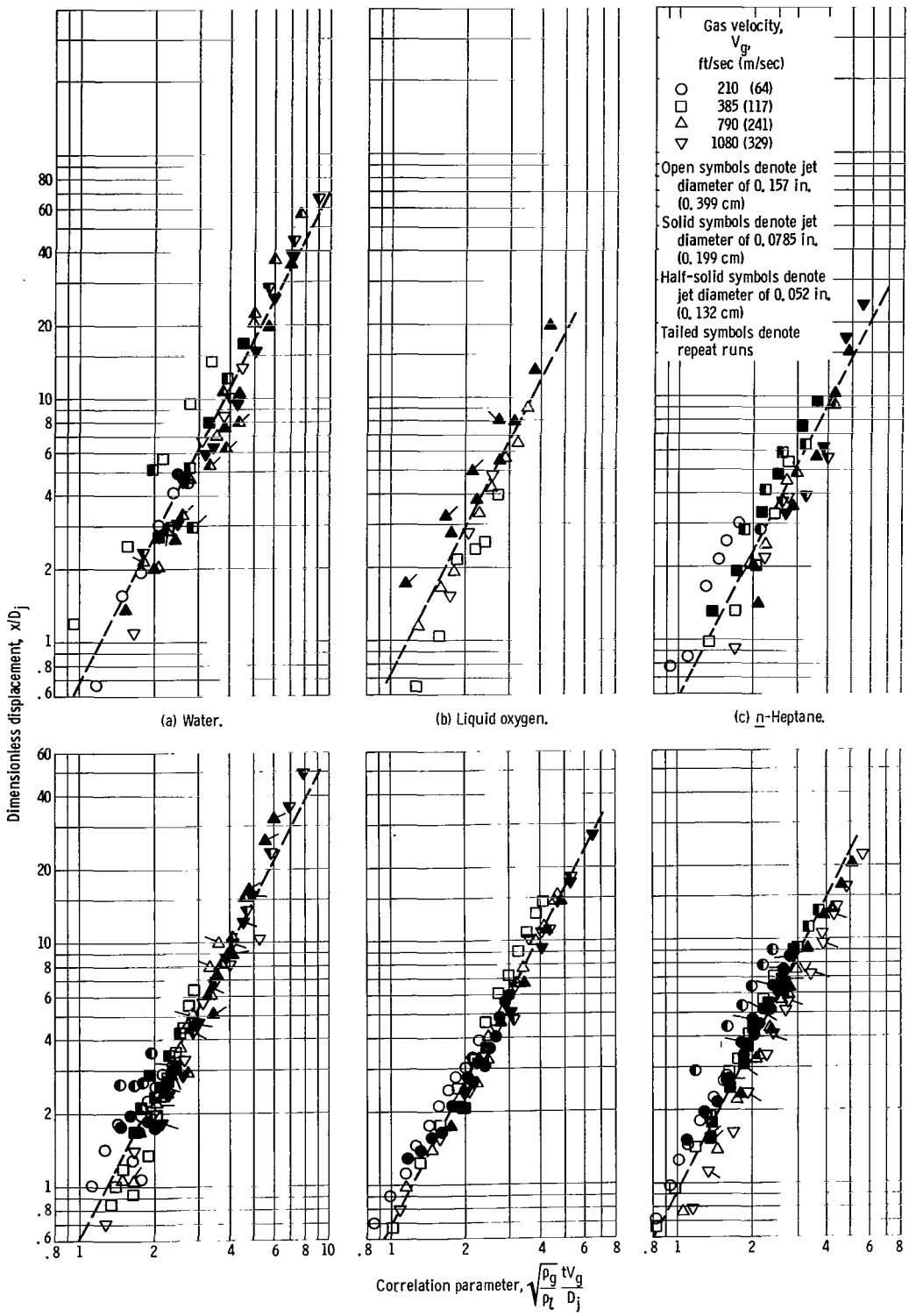

Figure 7. - Dimensionless jet displacement correlated with time, gas velocity, jet diameter, and density ratio.

$$\frac{x}{D_j} = C\left(\sqrt{\frac{\rho_g}{\rho_l}}\,\frac{tV_g}{D_j}\right)^2 \tag{1}$$

This equation corresponds to an expression derived for jet displacement with no mass loss assumed, as detailed in the appendix.

The data are plotted against the correlation parameter $\left(\sqrt{\rho_g/\rho_l}\right)tV_g/D_j$ in figure 7 for the six fluids. Lines with a slope of 2 faired through the data yield values for C from 0.58 for n-heptane to 0.92 for 79 percent glycerol and an average value of 0.70. Thus an empirically obtained expression for jet displacement is

$$\frac{x}{D_j} = 0.70\left(\sqrt{\frac{\rho_g}{\rho_l}}\,\frac{tV_g}{D_j}\right)^2 \tag{2}$$

Measured x/D_j is plotted against x/D_j calculated from equation (2) in figure 8. The dashed line represents equivalence of measured and calculated displacements. Although the scatter about this line is appreciable, the empirical displacement equation appears to predict the overall displacement trend accurately. In using figures 7 or 8 to estimate displacement with time for the fluids shown or for other fluids, it must be kept in mind that the time must not exceed the breakup time. Displacement of the jet reduced to ligaments or drops would be larger than that of the intact jet. Breakup times may be calculated for any particular set of conditions from equation (4) of reference 4.

A simple model of jet displacement as a function of time which accounts for mass loss from the jet is given in the appendix. Displacements calculated from the model are plotted against experimentally measured displacements in figure 9. The trend of displacement and the amount of scatter appear to be about the same regardless of whether mass loss is considered. Thus in application, displacements can be estimated from the simpler expression obtained empirically (eq. (2)).

The data of reference 7 for water jets displacing under the influence of a uniform gas velocity behind a shock wave are plotted against the empirical correlation parameter in figure 10. The average for water data from figure 7(a) is also shown. The data of reference 7 tend to have slightly greater displacements with time than the water data of this report but still within the scatter of all data shown in figure 8.

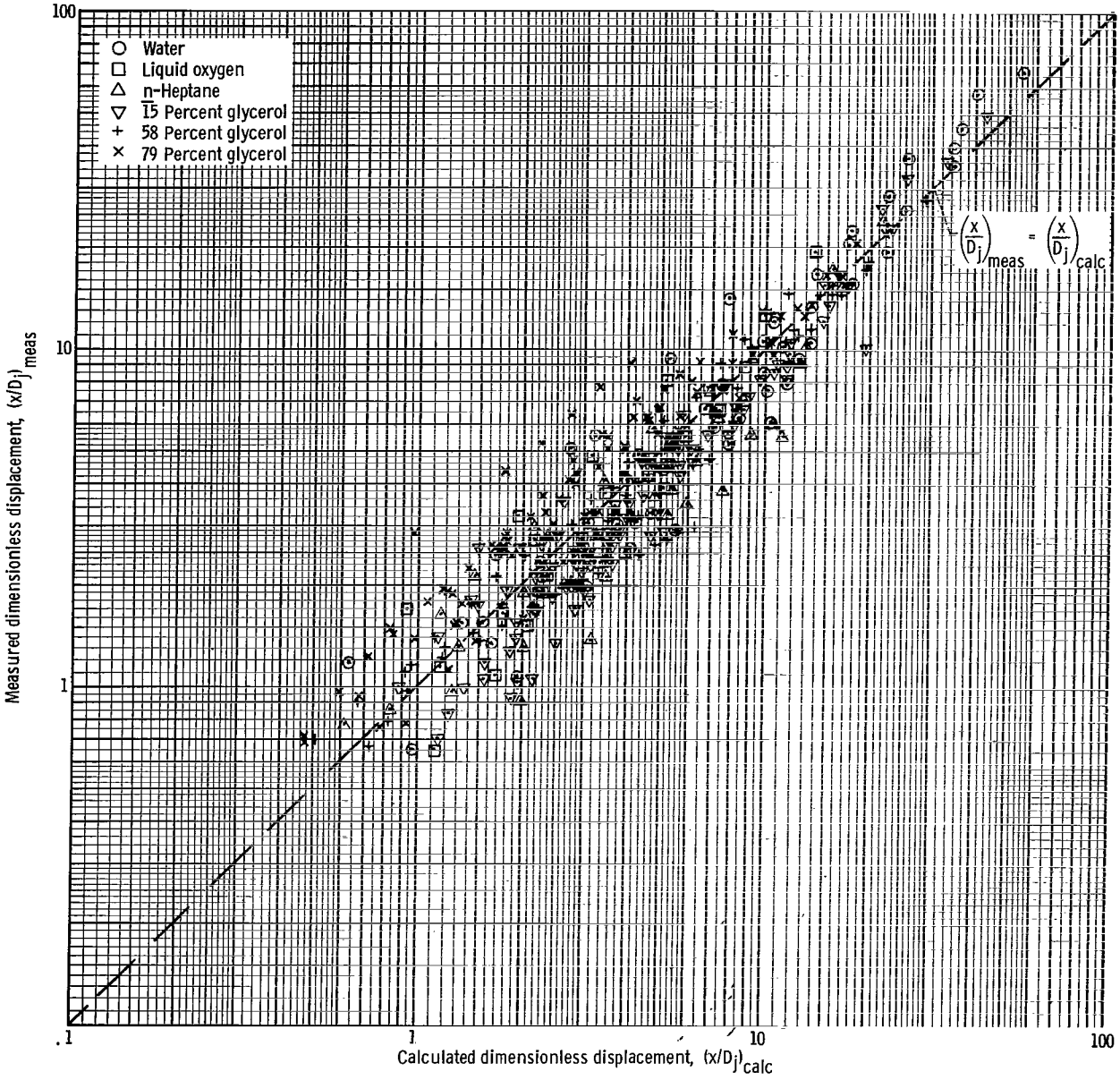

Figure 8. - Comparison of measured dimensionless displacements with values calculated from equation (2):

$$\frac{x}{D_j} = 0.70\left(\sqrt{\frac{\rho_g}{\rho_l}}\frac{tV_g}{D_j}\right)^2$$

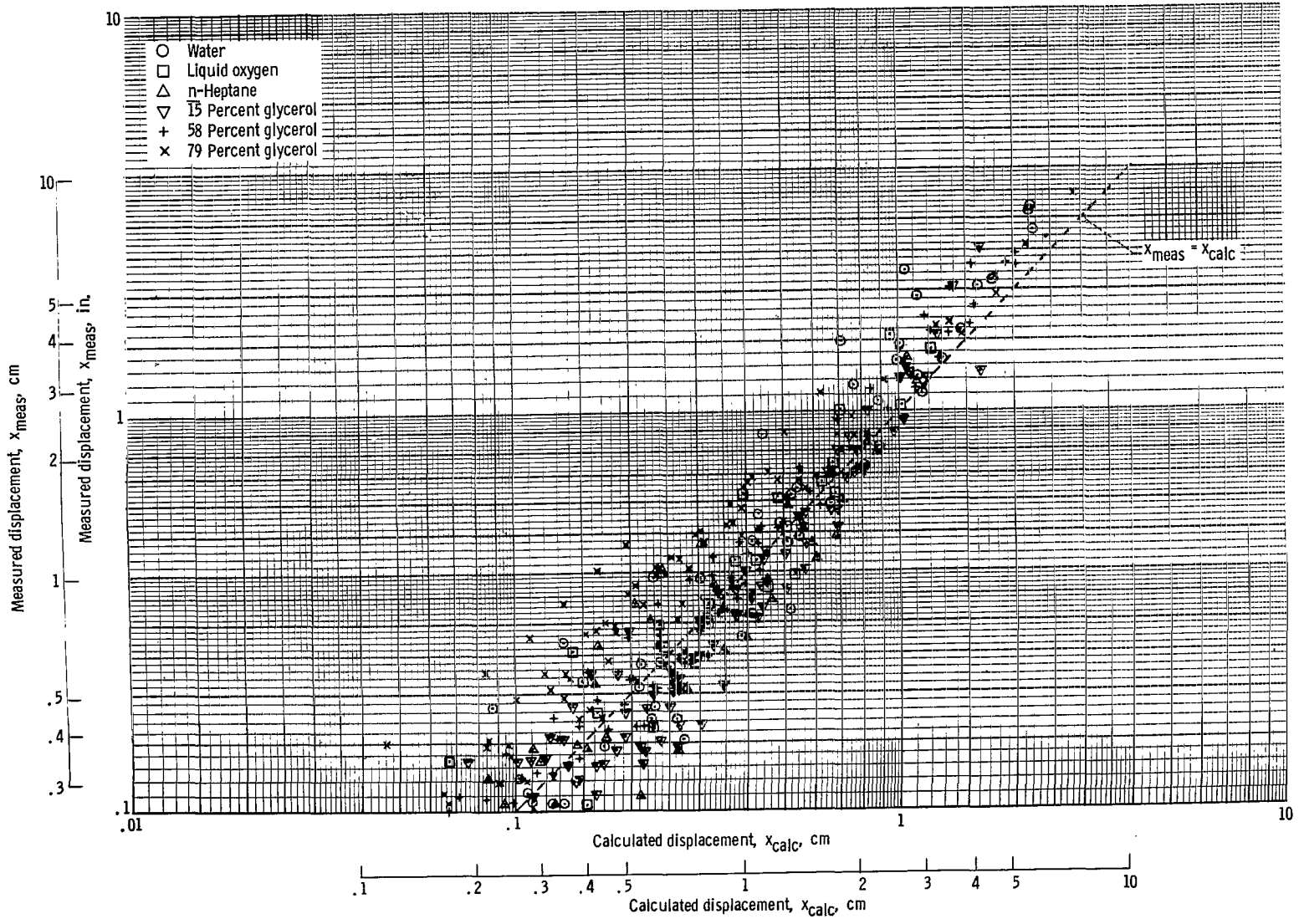

Figure 9. - Comparison of measured displacements with values calculated from equation (A5):

$$x_{calc} = V_g t + \frac{D_j}{2\alpha}\left(1 - \sqrt{1 - \frac{t}{t_b}}\right) - \frac{D_j\left(\frac{D_j}{4} + \beta\right)}{2\alpha\beta} \ln\left[\frac{4\beta}{D_j}\left(1 - \sqrt{1 - \frac{t}{t_b}}\right) + 1\right]$$

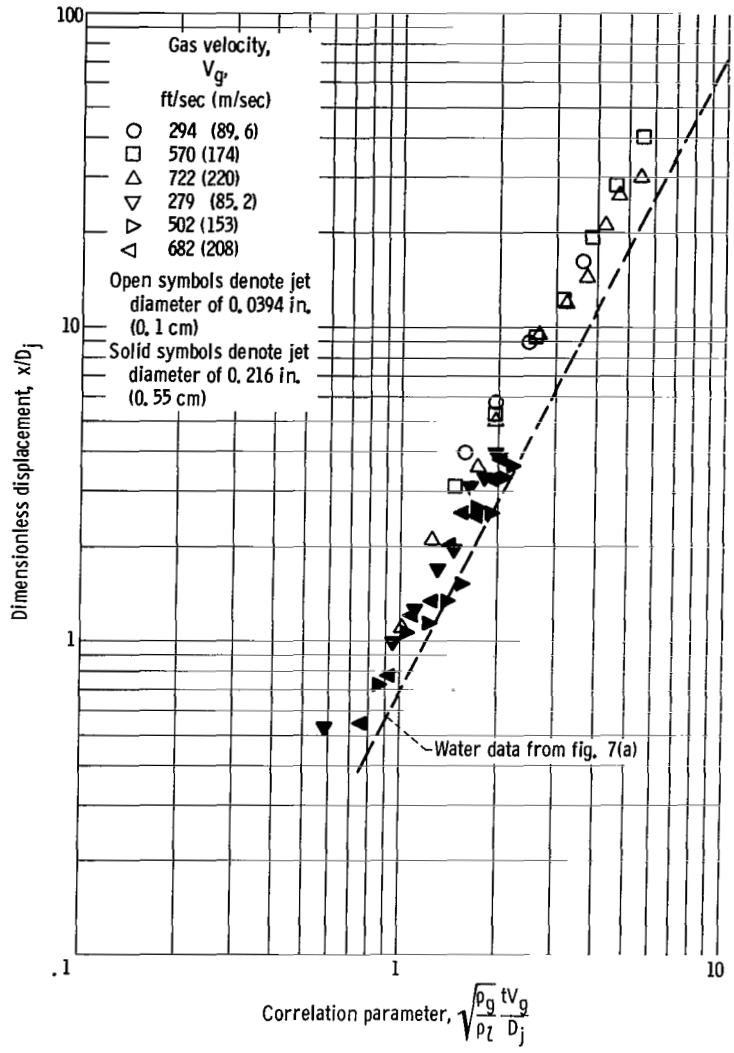

Figure 10. - Data of reference 7 as function of correlation parameter.

SUMMARY OF RESULTS

Jet displacements in a transverse gas flow were measured in a shock tube for three sizes of jets of water, n-heptane, and liquid oxygen and three glycerol-water mixtures. In all cases the displacement was approximately proportional to the gas velocity squared and inversely proportional to the jet diameter. The fluid properties had little effect on displacement.

Experimental displacement data were correlated with an empirically obtained parameter which includes time, liquid jet diameter, crossflow gas velocity, and the ratio of gas to liquid densities. Reasonably good agreement was obtained for all fluids. Sim-

ilar data for water jets taken independently also show fair agreement with the correlation parameter.

A simple model of jet displacement which includes the rate of mass removal correlates the data equally well. This model can be shown to suggest the empirical correlation parameter.

Lewis Research Center,
National Aeronautics and Space Administration,
Cleveland, Ohio, September 14, 1967,
128-31-06-02-22.

APPENDIX - MODEL OF JET DISPLACEMENT

The model presented is an attempt to suggest a correlating parameter for displacement of disintegrating liquid jets. The model accounts for mass loss and deformation of the jet cross section during the displacement.

In developing the force balance on a disintegrating jet, the initial circular jet cross section is assumed to deform upon impact of the shock wave to a segment of a larger circle (ref. 9) as shown in the sketch.

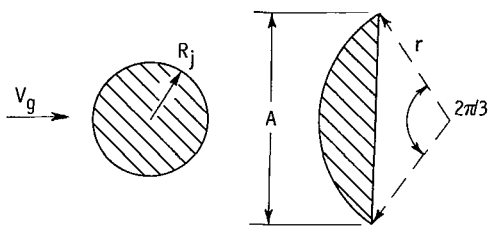

Photographic evidence of such a shape is shown in reference 6. In reality, it would take some finite time for this new cross section to develop. The equilibrium included angle $2\pi/3$ was selected as a lower limit based on measured pressure coefficients for a cylinder in a crossflow (ref. 10); that is, the end points of the segment correspond to points where the static pressure is a minimum. For the assumed shape,

$$\text{Cross-sectional area} = \frac{1}{2} r^2 \left(\frac{2\pi}{3} - \sin \frac{2\pi}{3} \right) = \frac{M}{\rho_l} \tag{A1}$$

From geometry the frontal area per unit length of jet is

$$A = 2.21 \sqrt{\frac{M}{\rho_l}} \tag{A2}$$

If surface tension and shear effects are neglected, the force balance per unit length of jet in a crossflow of velocity V_g may be written as

$$M \frac{d^2x}{dt^2} = \frac{1}{2} \rho_g C_D A \left(V_g - \frac{dx}{dt} \right)^2 \tag{A3}$$

In order to solve equation (A3) two additional assumptions were made:

(1) The rate of mass removal is the average value M_0/t_b, so that

$$M = M_0\left(1 - \frac{t}{t_b}\right)$$

(2) The drag coefficient C_D is constant. (The frontal area per unit length A varies.)

The introduction of these assumptions yields

$$R_j\left(1 - \frac{t}{t_b}\right)^{1/2}\frac{d^2x}{dt^2} = 0.623\,\frac{\rho_g}{\rho_l}\,C_D\left(V_g - \frac{dx}{dt}\right)^2 \tag{A4}$$

which can be integrated to give

$$x = V_g t + \frac{D_j}{2\alpha}\left(1 - \sqrt{1 - \frac{t}{t_b}}\right) - \frac{D_j\left(\frac{D_j}{4} + \beta\right)}{2\alpha\beta}\ln\left[\frac{4\beta}{D_j}\left(1 - \sqrt{1 - \frac{t}{t_b}}\right) + 1\right] \tag{A5}$$

where

$$\alpha = 0.623\,\frac{\rho_g}{\rho_l}\,C_D$$

and

$$\beta = \alpha V_g t_b$$

For the range of Reynolds numbers encountered in this study, the drag coefficient varies from 0.8 to 1.2 for a cylinder and is 1.1 for a disk (ref. 11). For convenience, a value of 1.0 was selected for use in equation (A5).

If the breakup time is assumed to have no effect (or mass loss is unimportant), dx/dt is small compared with V_g, and C_D remains constant, then equation (A4) reduces to

$$\frac{d^2x}{dt^2} = 2\alpha \frac{V_g^2}{D_j} \tag{A6}$$

which integrates to

$$\frac{x}{D_j} = 0.623\, C_D \left(\sqrt{\frac{\rho_g}{\rho_l}}\, \frac{tV_g}{D_j} \right)^2 \tag{A7}$$

Equation (A7) is equivalent to equation (2) for $C_D = 1.12$, which appears reasonable.

REFERENCES

1. Priem, Richard J.; and Morrell, Gerald: Application of Similarity Parameters for Correlating High-Frequency Instability Behavior of Liquid Propellant Combustors. Detonation and Two-Phase Flow. Vol. 6 of Progress in Astronautics and Rocketry. Academic Press, Inc., 1962, pp. 305-320.

2. Morrell, G.: Breakup of Liquid Jets by Transverse Shocks. Eighth Symposium (International) on Combustion. The Williams & Wilkins Co., 1962, pp. 1059-1068.

3. Morrell, Gerald: Rate of Liquid Jet Breakup by a Transverse Shock Wave. NASA TN D-1728, 1963.

4. Morrell, Gerald; and Povinelli, Frederick P.: Breakup of Various Liquid Jets by Shock Waves and Applications to Resonant Combustion. NASA TN D-2423, 1964.

5. Clark, Bruce J.: Breakup of a Liquid Jet in a Transverse Flow of Gas. NASA TN D-2424, 1964.

6. Engel, O. G.: Fragmentation of Waterdrops in the Zone Behind an Air Shock. J. Res., Nat'l. Bur. Standards, vol. 60, no. 3, Mar. 1958, pp. 245-280.

7. Muirhead, J. C.: Blast Wave Attenuation. Pt. I. Water Walls. Tech. Paper 175, Suffield Experimental Station, Defence Research Board (Canada), 1959.

8. Henshall, B. D.: On Some Aspects of the Use of Shock Tubes in Aerodynamic Research. R. & M. No. 3044, British A. R. C., 1957.

9. Taylor, Geoffrey I.: The Shape and Acceleration of a Drop in a High Speed Air Stream. Rep. No. Ptn/6600/5278/49, Chemical Defense Experimental Establishment (Gt. Brit.), 1956.

10. Roshko, Anatol: Experiments on the Flow Past a Circular Cylinder at Very High Reynolds Number. J. Fluid Mech., vol. 10, no. 3, 1961, pp. 345-356.

11. Prandtl, L.; and Tietjens, O. G. (J. P. Den Hartog, trans.): Applied Hydro- and Aeromechanics. Dover Publications, 1934 (reprinted 1957), pp. 97-100.

NASA-Langley, 1968 —— 33 E-4086

"The aeronautical and space activities of the United States shall be conducted so as to contribute . . . to the expansion of human knowledge of phenomena in the atmosphere and space. The Administration shall provide for the widest practicable and appropriate dissemination of information concerning its activities and the results thereof."

—NATIONAL AERONAUTICS AND SPACE ACT OF 1958

NASA SCIENTIFIC AND TECHNICAL PUBLICATIONS

TECHNICAL REPORTS: Scientific and technical information considered important, complete, and a lasting contribution to existing knowledge.

TECHNICAL NOTES: Information less broad in scope but nevertheless of importance as a contribution to existing knowledge.

TECHNICAL MEMORANDUMS: Information receiving limited distribution because of preliminary data, security classification, or other reasons.

CONTRACTOR REPORTS: Scientific and technical information generated under a NASA contract or grant and considered an important contribution to existing knowledge.

TECHNICAL TRANSLATIONS: Information published in a foreign language considered to merit NASA distribution in English.

SPECIAL PUBLICATIONS: Information derived from or of value to NASA activities. Publications include conference proceedings, monographs, data compilations, handbooks, sourcebooks, and special bibliographies.

TECHNOLOGY UTILIZATION PUBLICATIONS: Information on technology used by NASA that may be of particular interest in commercial and other non-aerospace applications. Publications include Tech Briefs, Technology Utilization Reports and Notes, and Technology Surveys.

Details on the availability of these publications may be obtained from:

SCIENTIFIC AND TECHNICAL INFORMATION DIVISION

NATIONAL AERONAUTICS AND SPACE ADMINISTRATION

Washington, D.C. 20546